INFLUENCE OF TOPOGRAPHY ON WIND PRESSURES IN TANKS USING CFD

O.A. FALCINELLI[†], S.A. ELASKAR[†,‡] and L.A. GODOY[†,‡]

[1]*Faculty of Exact, Physical and Natural Sciences, National University of Córdoba*
P. O. Box 916, Córdoba 5000, Argentina. lgodoy@com.uncor.edu
‡*CONICET*

***Abstract* — The influence of topography on wind pressures acting on structures has been of interest to the civil engineering community for some time; however, because of the complexity of the problem, only few cases have been solved. The evaluation of pressures in tanks located in hills is one of those complex problems and has not been addressed in the literature. This paper presents a computational fluid dynamics simulation of the problem, in which the domain including the hill and the tank is discretized using finite elements. The results show that the actual location of the tank with respect to a hill has a significant influence on the pressures, so that tanks located at the top of a hill undergo severe increases in pressure coefficients and also changes in pressure distributions around the tank.**

***Keywords*— CFD, finite elements, tanks, topographic effects, wind pressures**

I. INTRODUCTION

This paper addresses the computational modeling of wind pressures acting on the cylindrical part and on the roof of storage tanks, which are placed at different locations with respect to a hill. Wind pressures on above ground steel storage tanks may be evaluated by means of boundary layer wind tunnel (BLWT) simulations, or by computational techniques using computational fluid dynamics (CFD). Both methodologies have experimented considerable improvements over the past few years, so that advances in computing power, electronic instrumentation and computer-based rapid prototyping have improved the efficiency of BLWT simulations, whereas CFD models have benefited from computing power and improved software. There are still several advantages in using BLWT over CFD simulations, especially whenever the flow is dominated by turbulence, as in the present case. However, BLWT facilities are not available in most academic laboratories (even less so in developing countries) and those that have the facilities tend to be overloaded. Thus, CFD models are a useful tool to obtain estimates of pressures in structural configurations with reasonable costs. This paper addresses such situation, in which the influence of topographic effects on wind loaded tanks is of interest.

The importance of taking into account the influence of topography to estimate wind pressures has been recognized for some time in the context of civil engineering structures. Current codes of practice, such as the ASCE 7 (2006) provisions, include factors to account for the location of a structure with respect to hills and escarpments. Topographic factors relate wind velocities in open terrain with velocities at specific locations in a geographic accident (Jackson and Hunt, 1975; Lemelin *et al.,* 1988); however, considering the way in which they are formulated, those factors appear to be independent of the specific structure under study. For more complex situations, the ASCE document recommends the use of engineering judgment, expert advice, or wind tunnel studies. This work explores an alternative in which a computer simulation of the problem is carried out using computational fluid dynamics and the finite element method.

There are several CFD and wind tunnel studies performed on different hill types as well as on isolated tanks, but not the two taken in conjunction. Regarding wind loads on tanks, the most important reference known to the authors is the study in three parts reported by Macdonald *et al.* (1988, 1990a, 1990b), in which wind tunnel measurements were carried out for isolated tanks, and also for groups of tanks. Macdonald and coworkers also discussed the problems faced in representing Reynolds numbers using similitude theory for low-rise structures. Another class of open top tanks was addressed in the literature by Holroyd (1983). The flow over hills has been studied by several researchers using CFD, including Bergeles (1985), Taylor (1998), Kim *et al.* (2000), Lun *et al.* (2003) and Bitsuamlak *et al.* (2006). Most researchers model a two dimensional domain; however, a three-dimensional volume is needed in the present case because the presence of the tank in the hill destroys the plane condition.

Section II in this work contains the general fluid dynamics formulation of the problem. The computational model to simulate the air flow around a structure which is located in a hill, based on a general-purpose finite element code, is explained in Section III. The model is validated in Section IV by comparison with the results of two benchmarks originally solved by other authors. Results of the flow for an isolated tank located on a horizontal plane are given in Section V; whereas Section VI reports new results that include both a hill and the structure.

II. BASIC FLUID DYNAMICS FORMULATION

The planetary boundary layer near ground is simulated in this paper under the assumptions of stationary mean flow, viscous, incompressible, isothermal, and turbulent

flow. The problem is governed by four sets of conditions: First, the continuity equation may be written in the form Brun *et al.* (1959)

$$\frac{\partial U}{\partial x}+\frac{\partial V}{\partial y}+\frac{\partial W}{\partial z}=0 \tag{1}$$

where *U, V, W* are the velocity components, and ρ is the density of the fluid. Second, the Reynolds equations are:

$$\rho\frac{\partial U}{\partial t}+\rho U\frac{\partial U}{\partial x}+\rho V\frac{\partial U}{\partial y}+\rho W\frac{\partial U}{\partial z}= \rho g_x-\frac{\partial P}{\partial x}+\frac{\partial}{\partial x}\left[2(\mu+\mu_t)\frac{\partial U}{\partial x}\right]+ \frac{\partial}{\partial y}\left[(\mu+\mu_t)\left(\frac{\partial U}{\partial y}+\frac{\partial V}{\partial x}\right)\right]+\frac{\partial}{\partial z}\left[(\mu+\mu_t)\left(\frac{\partial U}{\partial z}+\frac{\partial W}{\partial x}\right)\right] \tag{2.a}$$

$$\rho\frac{\partial V}{\partial t}+\rho U\frac{\partial V}{\partial x}+\rho V\frac{\partial V}{\partial y}+\rho W\frac{\partial V}{\partial z}= \rho g_y-\frac{\partial P}{\partial y}+\frac{\partial}{\partial x}\left[(\mu+\mu_t)\left(\frac{\partial U}{\partial y}+\frac{\partial V}{\partial x}\right)\right]+ \frac{\partial}{\partial y}\left[2(\mu+\mu_t)\frac{\partial V}{\partial y}\right]+\frac{\partial}{\partial z}\left[(\mu+\mu_t)\left(\frac{\partial V}{\partial z}+\frac{\partial W}{\partial y}\right)\right] \tag{2.b}$$

$$\rho\frac{\partial W}{\partial t}+\rho U\frac{\partial W}{\partial x}+\rho V\frac{\partial W}{\partial y}+\rho W\frac{\partial W}{\partial z}= \rho g_z-\frac{\partial P}{\partial z}+\frac{\partial}{\partial x}\left[(\mu+\mu_t)\left(\frac{\partial U}{\partial z}+\frac{\partial W}{\partial x}\right)\right]+ \frac{\partial}{\partial y}\left[(\mu+\mu_t)\left(\frac{\partial V}{\partial z}+\frac{\partial W}{\partial y}\right)\right]+\frac{\partial}{\partial z}\left[2(\mu+\mu_t)\frac{\partial W}{\partial z}\right] \tag{2.c}$$

where μ is viscosity; μ_t is the turbulent viscosity, g_x, g_y, g_z are the gravity components and *P* is the pressure.

Third, the conditions arising from the Boussinesq hypothesis should be satisfied, in which the turbulent viscosity μ_t is related to the turbulent kinetic energy *K* and its dissipation ε:

$$\mu_t=C_\mu\,\rho\,\frac{K^2}{\varepsilon} \tag{3}$$

where C_μ is an empirical parameter.

Fourth, the classical *K*-ε turbulent flow model provides the conditions of conservation and dissipation of turbulent kinetic energy in the form:

$$\rho U\frac{\partial K}{\partial x}+\rho V\frac{\partial K}{\partial y}+\rho W\frac{\partial K}{\partial z}=\frac{\partial}{\partial x}\left[\left(\frac{\mu_t}{\sigma_K}+\mu\right)\frac{\partial K}{\partial x}\right]+ \frac{\partial}{\partial y}\left[\left(\frac{\mu_t}{\sigma_K}+\mu\right)\frac{\partial K}{\partial y}\right]+\frac{\partial}{\partial z}\left[\left(\frac{\mu_t}{\sigma_K}+\mu\right)\frac{\partial K}{\partial z}\right]-\rho\varepsilon+ \mu_t\left[\begin{array}{l}2\left(\frac{\partial U}{\partial x}\right)^2+2\left(\frac{\partial V}{\partial y}\right)^2+2\left(\frac{\partial W}{\partial z}\right)^2+\left(\frac{\partial U}{\partial y}+\frac{\partial V}{\partial x}\right)^2+\\ \left(\frac{\partial U}{\partial z}+\frac{\partial W}{\partial x}\right)^2+\left(\frac{\partial V}{\partial z}+\frac{\partial W}{\partial y}\right)^2\end{array}\right] \tag{4.a}$$

$$\rho U\frac{\partial \varepsilon}{\partial x}+\rho V\frac{\partial \varepsilon}{\partial y}+\rho W\frac{\partial \varepsilon}{\partial z}=\frac{\partial}{\partial x}\left[\left(\frac{\mu_t}{\sigma_\varepsilon}+\mu\right)\frac{\partial \varepsilon}{\partial x}\right]+ \frac{\partial}{\partial y}\left[\left(\frac{\mu_t}{\sigma_\varepsilon}+\mu\right)\frac{\partial \varepsilon}{\partial y}\right]+\frac{\partial}{\partial z}\left[\left(\frac{\mu_t}{\sigma_\varepsilon}+\mu\right)\frac{\partial \varepsilon}{\partial z}\right]-C_2\rho\frac{\varepsilon^2}{K}+ C_1\mu_t\frac{\varepsilon}{K}\left[\begin{array}{l}2\left(\frac{\partial U}{\partial x}\right)^2+2\left(\frac{\partial V}{\partial y}\right)^2+2\left(\frac{\partial W}{\partial z}\right)^2+\\ \left(\frac{\partial U}{\partial y}+\frac{\partial V}{\partial x}\right)^2+\left(\frac{\partial U}{\partial z}+\frac{\partial W}{\partial x}\right)^2+\left(\frac{\partial V}{\partial z}+\frac{\partial W}{\partial y}\right)^2\end{array}\right] \tag{4.b}$$

where C_1, C_2, C_μ, σ_K and σ_ε are experimental parameters. Values of C_1 = 1.44, C_2 = 1.92, C_μ =0.09, σ_K = 1 and σ_ε = 1.3 have been used in this paper, as suggested in the literature (CFDesign, 1999).

III. COMPUTATIONAL MODEL

The fluid dynamics computations required to model atmospheric flows around hills and tanks were carried out in this research using the general purpose finite element package NASTRAN CFDesign (1999). However, several features of the model need to be calibrated before it can be employed with confidence in the field of tanks.

A. On the computational modeling of atmospheric flows

Any wind flow model in the planetary boundary layer (either computational or wind tunnel model) faces the need for a strategy to stabilize the evolution of the velocity profile which is considered to be adequate for the specific problem under study. In wind tunnel experiments, good results have been obtained by imposing a controlled roughness on the floor of the tunnel (Maher, 1966; Macdonald *et al.*, 1998; Portela and Godoy 2005a). This has also been effective in some computational models; however, the specific software used in this research can only apply the same roughness conditions to all surfaces with a boundary condition involving zero velocity. This means that a roughness condition imposed on the floor would also be imposed on the walls of the tank. Furthermore, the value of the geometric parameter required to get a stable evolution of the velocity profile is of comparable magnitude to a characteristic length of the problem, i.e. the actual diameter of the tank, so that the computed pressure field would be significantly affected, leading to incorrect predictions of the results (Cheung and Melbourne 1983).

There is an alternative way in which the atmospheric velocity profile can be stabilized, in which the size of the first row of elements (adjacent to the floor) is taken as a stabilizing parameter. This technique attempts to modify the shear stresses between the external flow and the floor (and thus modify the velocity profile) by means of a different turbulent model, which imposes a wall law in the first row of elements. Such strategy was previously explored and used by the authors (Falcinelli *et al.*, 2003) and provided excellent results with respect to known values obtained from the literature.

In the *k*-ε turbulence model that is used in the computer code CFDesign, the velocity within the lower layers in the boundary layer is not computed during the analysis, but it is imposed according with a given law. This "wall law" models the velocity using a logarithmic profile and is prescribed on the first row of finite elements adjacent to the solid boundary. Thus, the size given to the first element in the vertical direction becomes important, because it is related with the size of the lower layers. It is not simple to fix the size of the first row of elements *a priori* (i.e. before performing the computations), so that an *a posteriori* approach has been carried out in this work, in which the quality of the solu-

tion is assessed for several element sizes in the first row. Thus, the atmospheric flow is modeled as an external flow and the stability in the velocity profile is reached by modifying the shear stress on the floor surface through the modification of the size of the first element adjacent to the boundary.

B. Problems related with the presence of high Reynolds numbers

The relative height of the boundary layer may have a strong dependence on the Reynolds number, so that an increase in the latter is associated with a decrease in the former. The consequence of this interdependence for the computational model is that those elements used to model viscous zones should be smaller in size with respect to the characteristic length of the flow for large Reynolds numbers, and vice versa. But the ratio of maximum distortion of the elements is limited by computational constraints, so that a decrease in height should also be accompanied by a decrease in the other dimensions. Thus, an increase in the Reynolds number leads to an increase in the number of elements required to carry out the discretization of the solid surfaces, and consequently leads to an increase in the size of the element meshes. A consequence of the above is that the computational resources available to perform the present computations are a constraint on the values of the Reynolds numbers that can be modeled.

For the tanks and wind conditions of interest, typical Reynolds numbers are 1.28×10^8; however, the use of personal computers (as in this research), limits the maximum Reynolds number that can be modeled to about 1/10 of that value (approximately 1.28×10^7). Because of that, several authors (Mulhearn *et al.*, 1976; Finnigan and Longstaff, 1982; Cheung and Melbourne, 1983; Macdonald *et al.*, 1998) use the hypothesis that "the wall pressure distribution may be assumed to be independent of the Reynolds number if the test Reynolds number exceeds 1×10^5 " (Macdonald *et al.*, 1998).

Several cases were modeled in this research, using Reynolds numbers of 1/20, 1/30, and 1/40 of the expected full scale value, and it was found that the pressure fields do not show significant differences neither qualitative nor quantitative (differences were lower than 3%) (Falcinelli *et al.*, 2003). The conclusion is that the present results are expected to be reasonably accurate even though there are differences between the expected and assumed Reynolds numbers.

C. K-ε Model

The turbulence model known as K-ε (see Eq. 4), which is available in CFDesign, has been adopted in this work. The model has been incorporated in the CFDesign code for some time and has gone through a number of tests, so that one may be confident in the robustness of the turbulent model implementations to solve engineering problems involving turbulent flows (CFDesign, 1999). Notice that the present research is limited to the evaluation of pressure distributions acting on tanks in different topographic locations and is not concerned with the evaluation of the various available models for the simulation of atmospheric turbulence. Validation of the model has been made using two different benchmarks.

D. Parameters adopted for the analyses

The parameters needed to reach a stable atmospheric boundary layer were defined during the process of the research. This was first done for a two-dimensional domain and it was later extended to three dimensions. The results obtained from 2D models were compared with those given by ASCE 7 (2006) using the parameters identified to obtain a stable velocity profile. Then, 3D models were investigated, in which a tank was placed at different locations with respect to a hill.

The physical control volumes used are large domains, with the consequence that a large number of finite elements is necessary to simulate the flow inside the control volume. Because of the symmetry assumed in the problem, it was only necessary to consider half of the domain, with element meshes covering 1,100m in elevation, 800m in width, and 1,000m before and after the top of the hill. At the entrance to the control volume, a logarithmic velocity profile was imposed following ASCE 7, in the form

$$u = v_h \cdot ln\left(\frac{z}{z_0}\right) \tag{5}$$

where u is the velocity component in the direction of incidence of the flow; v_h is a reference velocity (needed to adjust the intensity of the incident flow); z is the elevation with respect to ground level; and z_0 is a constant used to normalize the elevation. In the present problem, values of $z_m = 0.002059m$ and $v_k = 7.6378m/s$ were used to fit the 2D data of the ASCE provisions. The density of the fluid was assumed as $\rho = 1.2047Kg/m^3$, whereas the dynamic viscosity was adopted as $\mu = 0.00035N.s/m^2$. This choice of dynamic viscosity was made in order to avoid problems related with high Reynolds numbers (see Section 3.2).

The boundary conditions for the 3D model (illustrated in Fig. 1) were prescribed velocity on the front and top surfaces of the control volume following Eq. (5); prescribed pressure on the back surface (reference pressure); zero velocity at the bottom and at the body surface; and a condition of no penetration was applied on both lateral planes to account for symmetry.

The values of turbulent kinetic energy are prescribed at the entrance of the control volume. In the CFDesign code, the kinetic energy is computed as $K = 0.5\cdot(\overline{u^2}+\overline{v^2}+\overline{w^2})$, where $\overline{u^2}$, $\overline{v^2}$ and $\overline{w^2}$ are the mean square of the turbulent perturbation associated with the velocities in the x, y, z directions. The mean value of the velocity intensity is computed as a factor of turbulence intensity multiplied by the mean value of the velocity in each direction $I = \sqrt{\overline{u^2}}/|U| = \sqrt{\overline{v^2}}/|V| = \sqrt{\overline{w^2}}/|W|$. The factor of turbulence intensity adopted in this work was 1%.

The boundary conditions imposed on the turbulent kinetic energy and its dissipation ε are a zero gradient

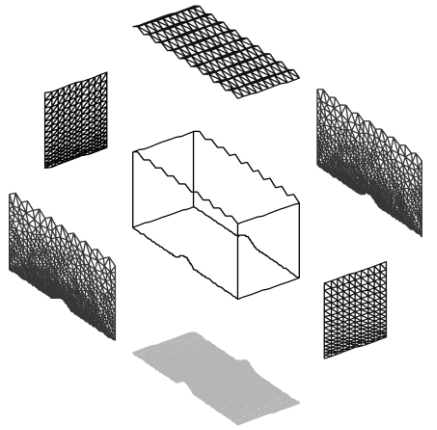

Figure 1. Boundary conditions. Front and top surfaces: prescribed velocity using Eq. (5). Bottom surface: zero velocity. Back: prescribed pressure. Lateral: symmetric conditions.

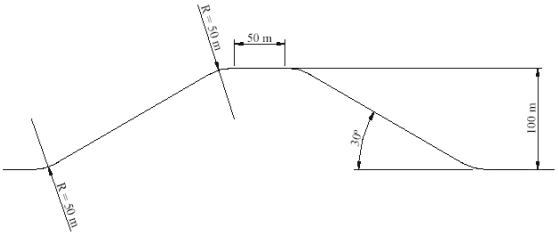

Figure 2. Topographic accident modeled in this work.

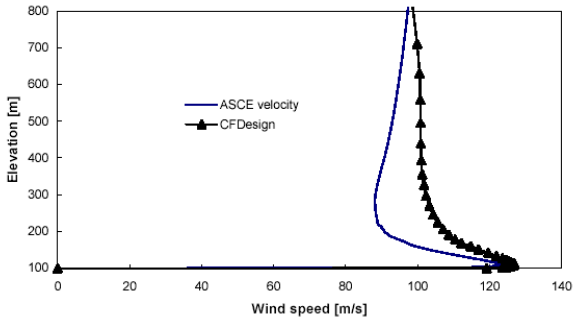

Figure 3. Wind velocity profiles computed in this work and as specified by ASCE 7.

in the direction perpendicular to the surface at the exit of the control volume and on the symmetry planes. At the entrance to the control volume, a value $\varepsilon = C_\mu K^{1.5} / \delta_S$ is specified, where C_μ is the constant used in Eq. 4.b, and δs is the mix length, which was assumed as 0.1*m* in this work. On the solid boundaries there are no constraints on the kinetic energy and its dissipation, since the wall law is specified. A sensitivity study was performed on the turbulence intensity factor and it was found that the variable did not lead to significant changes in the results (Falcinelli *et al.*, 2002; Falcinelli, 2004).

The results are presented in non-dimensional form. Notice that for this type of flow, there is no characteristic velocity which could be used to obtain non-dimensional quantities, because the velocity is a function of elevation. The pressures computed are relative values since the reference pressure may be different from one model to another. However, because the flow is incompressible, a change in the reference pressure can be made whenever the results need to be compared.

E. Calibration of element size

It was necessary to identify the size of the first element adjacent to the ground in order to obtain velocity profiles similar to those given by ASCE on a hill. The comparison between the present model and the ASCE values gave rise to the problem that ASCE considers the perturbation produced by a generic topographic object with a given ratio height/length, but it does not specify other details regarding the shape of the topographic object. The results of a CFD simulation, on the other hand, show that there is sensitivity with respect to the shape of the topographic object. Furthermore, the specific geometry of the hills of interest in this work falls outside the range of values tabulated by ASCE. A procedure is explained in ASCE to compute a velocity profile with values of height/length outside the table, but the results are the same as those obtained using a geometry with a larger base (and with a very different ratio height/length). Thus, the results given by ASCE may only serve as an indication of an order of magnitude and not as an accurate value to be expected at a given elevation.

Several hill profiles were studied using the present CFD discretization. For a given height/length ratio, the velocity profiles depend on the parameters used to characterize the hill. The specific geometry considered in this investigation is defined by a 50*m* horizontal length for the top plateau of the hill, a 30º slope, and radius of curvature of 50m, as shown in Fig. 2. The resulting velocity profile is shown in Fig. 3, and it may be seen that the ASCE curve yields lower velocities, with a maximum difference of about 20%. For other geometries, the computed differences were of 5%. Thus, it seems that the present CFD model is capable of performing an adequate representation to the flow around a hill.

The velocity profile for a point located at the top of the hill (100*m* from the base of the hill) is plotted in Fig. 3. The size of the first row of elements adjacent to the floor in the finite element mesh was taken as 1.4*m* in all simulations; such element size was necessary to obtain a stable boundary layer in flat terrain and without perturbations.

F. Non-dimensional form of pressures

A non-dimensional form of pressures is usually defined by a pressure coefficient *Cp*, given by

$$Cp = \frac{p - p_{ref}}{\frac{1}{2} \cdot \rho \cdot v_{ref}^2} \qquad (6)$$

where p_{ref} is the static reference pressure; and the denominator is the dynamic reference pressure, given by the reference velocity v_{ref}. Both reference values (pressure and velocity) are extremely important in the normalization of the CFD results.

The conservation of energy of a particle may be considered by neglecting the change in gravitational potential energy (i.e., small changes in elevation), the internal

energy (assumption of isothermal flow), the compressibility effects (assumption of incompressible flow), and the work done by viscous stresses (assumption of low viscosity). Under those assumptions, the maximum pressure that may be attained by a particle which originally had (p_{ref}, v_{ref}) is the stagnation pressure p_0, given by

$$p_0 = p_{ref} + \frac{1}{2}\cdot\rho\cdot v_{ref}^2 \tag{7}$$

Such energy should remain constant along a stream line and measures the energy per unit volume of the particle. For each particle with velocity v the stagnation pressure may be computed in the form

$$p_0 = p + \frac{1}{2}\cdot\rho\cdot v^2 \Rightarrow p = p_0 - \frac{1}{2}\cdot\rho\cdot v^2 \tag{8}$$

so that the original pressure p may be evaluated using equation (8). This can be used to obtain pressures p of particles for which the pressure distribution p_0 at stagnation points are given.

In a cylindrical tank under wind flow, stagnation occurs at the windward meridian of the tank, so that the pressures can be obtained by means of equation (8). However, the assumption is required that a particle that reached the point of maximum pressure traveled at the same elevation (i.e., did not have vertical displacements).

Under this assumption, consider the stagnation pressure of a point located at an elevation z; then, the velocity of the particle before reaching the tank may be computed using the velocity profile imposed as a boundary condition:

$$v = 7.6378\frac{m}{s}\cdot ln\left(\frac{z}{0.002059m}\right) \tag{9}$$

The stagnation pressure is thus given by

$$p_0 = \bar{p} + \frac{1}{2}\cdot\rho\cdot\left[7.6378\frac{m}{s}\cdot ln\left(\frac{z}{0.002059m}\right)\right]^2 \tag{10}$$

where $\bar{p}$ is the pressure that a particle would have at the elevation z if a tank was not present, and is given by

$$\bar{p} = p_0 - \frac{1}{2}\cdot\rho\cdot\left[7.6378\frac{m}{s}\cdot ln\left(\frac{z}{0.002059m}\right)\right]^2 \tag{11}$$

In this research, the pressure $\bar{p}$ has been taken as a static reference pressure, i.e. $\bar{p} = p_{ref}$. The elevation z is taken as the elevation for which the maximum stagnation pressure was obtained.

The hypothesis about the horizontal traveling of a particle that reached the maximum pressure would perhaps be questionable for tanks located on a hill and some adjustments are in order. Thus, for an isolated tank it was necessary to identify the point for which the static pressure was the same as p_{ref}, and the resulting coordinates were at an elevation equal to 0.7 of the tank height and at a circumferential angle of 38º measured from the windward meridian. Finally, for each different location of a tank on a hill, the reference pressure p_{ref} was assumed as the static pressure at this point.

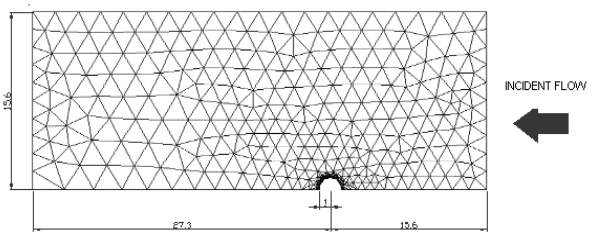

Figure 4. Element mesh employed in this work to compute the flow around a sphere.

The reference velocity employed in Eq. (6) is that obtained for a velocity profile without any topographic perturbation (Eq. 5) at 10m from ground level:

$$v_{ref} = 7.6378\frac{m}{s}\cdot ln\left(\frac{10m}{0.002059m}\right) \tag{12}$$

IV. VALIDATION OF THE COMPUTATIONAL MODEL

The methodology presented in the previous sections was validated by means of several studies of external flow to an object and for which known solutions were available. The first case presented in this section is the flow on a sphere in post-critical range (Re > 300,000), for which detached flow occurs. The second case is the flow around a tank in an atmospheric boundary layer investigated in wind tunnel experiments by Macdonald *et al*. (1998).

A. Post-critical flow around a sphere

A sphere with 1m diameter was considered under Re = 450,000; this is an axi-symmetric flow, so that two dimensional models can be employed. The plane investigated is shown in Fig. 4, and is at the intersection of the control volume and the axis of revolution of the sphere. The control volume is a cylinder in three dimensions; however, the domain investigated is only rectangular in 2D, with dimensions of 14.3 times the radius of the sphere in front of the object, 27.3 times behind the object, and 15.6 times in height. The finite element mesh contains 897 triangular elements and 503 nodes. The boundary conditions assumed are constant velocity at the entrance and at the top of the control volume; assumed pressure at the flow exit; symmetry at the side occupied by the sphere; and non-sliding condition on the sphere.

The distribution of Cp as a function of the angle (β) measured from the stagnation point is shown in Fig. 5, using both the present CFDesing and experiments reported by Brun *et al.* (1959). The results of pressures along the zone of detachment of the flow was modeled with only 30 elements on the sphere and showed very good agreement with the experimental values. Similar agreement was found in the zone of peak suctions and in the stagnation zone. The main differences are found in the position of the peak suctions (of about 8°). Note that this is a course mesh, and the actual location of the peak is corrected by a mesh refinement; however, good results of extreme (maximum and minimum) pressures are obtained even with a small number of elements. This case serves as an indication of the mesh refinement required to obtain meaningful values of Cp.

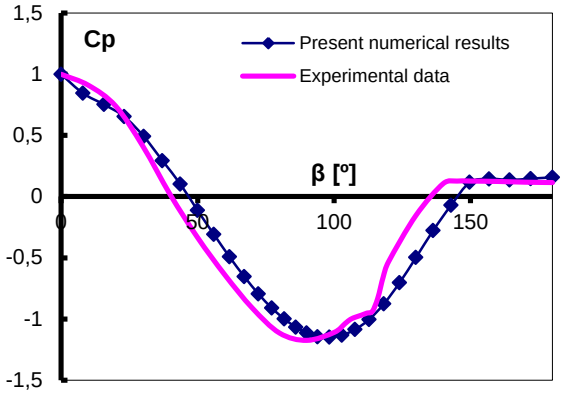

Figure 5. Computational and experimental pressure coefficients for the flow around a sphere. Experimental data from Brun et al. (1959).

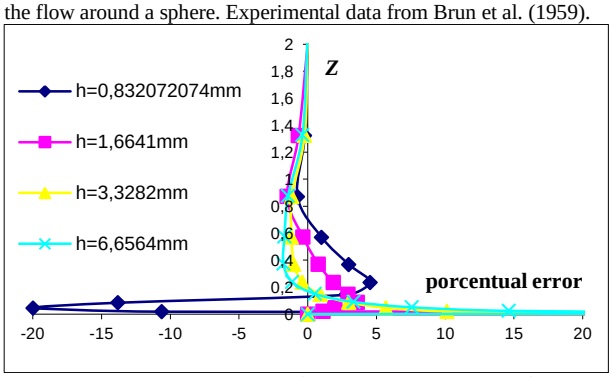

Figure 6. Error in the velocity profile computed at the exit of the control volume.

B. Simulation of the wind tunnel flow around a small scale silo

The second case considered is a wind tunnel test on a small scale silo immersed in an atmospheric flow, reported by Macdonald *et al*. (1998). The structure is similar to the structures of interest in this research, but it is located in a flat terrain. The velocity profile obtained in the tests is similar to that described by Eq. (5), with $v = w = 0$, in which v, w are the mean velocity components in the coordinate directions. The flow parameters in this case were v_h=2.54m/s and z_0=0.0002m.. The structure itself has 0.20m diameter and 0.20m height, with a conical roof slope of 25º.

The flow was first analyzed in a wind tunnel without the silo in order to calibrate the dimensions of the first layer of elements. Figure 6 shows the error at the exit of the computational domain considered, measured with respect to the profile imposed at the entrance. The results show that elements with 1.664mm in this case were able to produce a small distortion in the velocity profile, with errors of only 3.6%.

Using a stabilized velocity profile as described above, the next step was to generate a finite element mesh to model the flow around the silo. The control volume had to be meshed in such a way as to reproduce the external surface of the structure, shown in Fig. 7. The mesh shown in Fig. 8 has 213,630 elements and 38,370 nodes. The boundary conditions are specified velocity (according to Eq. 5) in all nodes of the front of the external surface of the control volume; specified pressure in the nodes of the back; free displacement in the plane of symmetry and no-slip on the floor and on the external surface of the silo.

The main results are presented in Figs. 9 and 10, with very good agreement with the experimental values reported in the literature (Macdonald *et al.* 1999). This case represents a useful validation of the stabilization procedure for the boundary layer employed in this paper.

V. WIND PRESSURES ON AN ISOLATED TANK

A theme tank, illustrated in Fig. 11, is used in this section to illustrate the pressure patterns in an isolated tank and the influence of a hill is considered in the next section. This geometry was previously used to carry out a comprehensive structural analysis under wind in several works (Godoy *et al.*, 2004; Portela and Godoy, 2005b; Sosa and Godoy, 2005). There is no full scale wind pressure data for this tank, or previous experimental or computational results of the influence of the topography

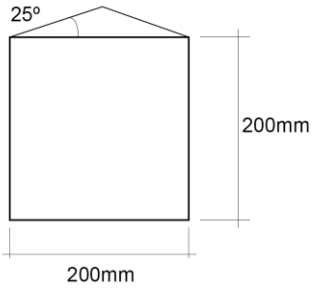

Figure 7. Dimensions of the small scale silo used as a benchmark

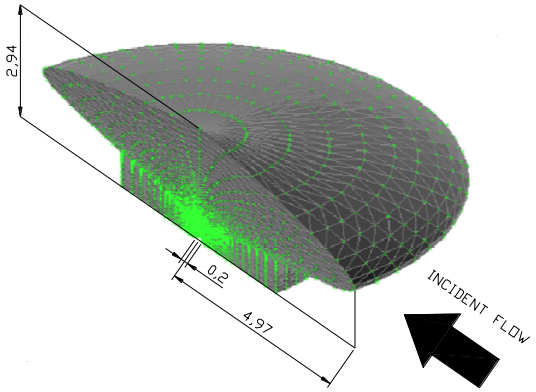

Figure 8. Mesh employed for the model of Fig. 7, in which the velocity profile is stabilized by means of the height of the elements adjacent to the floor. The dimensions are in meters.

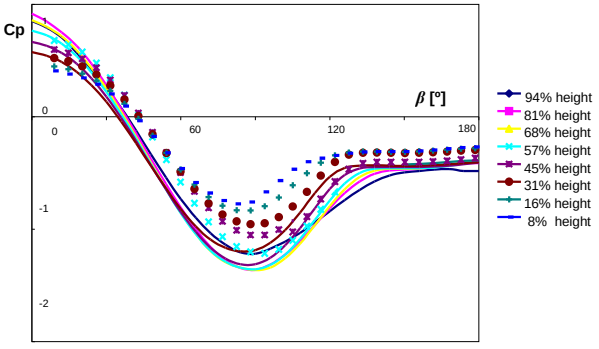

Figure 9. Pressure coefficients on silo walls calculated via CFD.

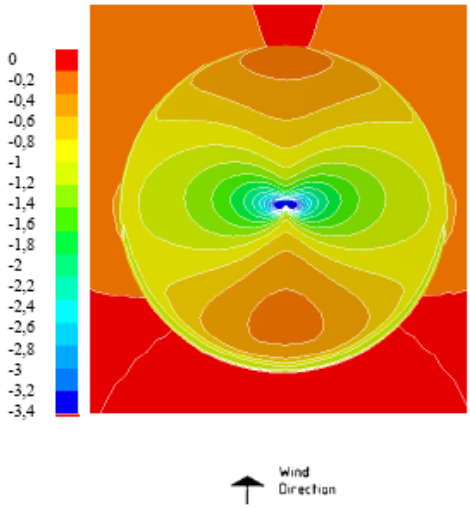

Figure 10. Pressure coefficients on the roof of a silo computed using CFD.

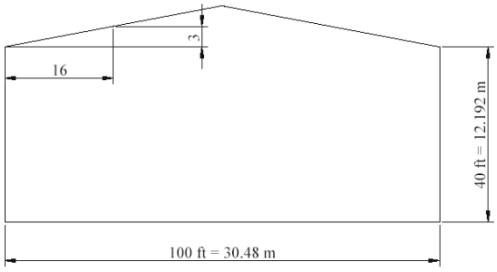

Figure 11 Geometry of the tank modeled.

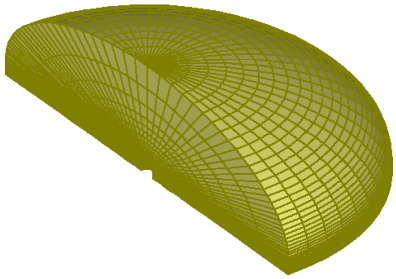

Figure 12. Fluid domain investigated, including hill and tank.

on wind pressures for tanks. The present model was built using tetrahedral elements, with a total of 28,320 elements and 29,088 nodes to discretize the fluid domain, as shown in Fig. 12. Studies were performed under different Reynolds numbers, and based on the numerical experiments it was decided to use a height of first element adjacent to the floor of 1.4*m*.

The pressures computed on the roof and on the cylinder of an isolated tank are shown in Fig. 13. The pressures were originally computed in *Pa*, but because this is an incompressible flow, the most important information is the change in pressures, so that the values can be normalized with respect to a reference pressure. In civil engineering applications, the pressures are normalized with respect to a value outside the structure itself.

On the leeward side of the tank, the results show low pressures under the junction between the cylinder and the roof; they are due to a vortex shedding as two flows cross, one which flows on the roof and another one is the detached flow on the leeward area.

The area covered by such low pressures is very small and can only be computed using a dense mesh of finite elements to capture the high pressure gradients induced. For this case, the pressures are qualitatively similar to those obtained by Macdonald *et al.* (1998), with some differences because the present model is shorter with respect to its diameter than the case studied by Macdonald and collaborators. Furthermore, the slope of the roof is different, with a larger slope in the case of Macdonald *et al.* (1998), so that vortex shedding is not present as in the present research. Another reference pressure distribution was obtained by Purdy *et al.* (1967) and they are similar to those shown in Fig. 13, but not completely comparable because the velocity profiles adopted are very different.

VI. WIND PRESSURES ON A TANK LOCATED ON A HILL

The results in this work are used to understand the influence of topographic features on the wind pressures in tanks. This study was motivated by a specific interest in which a new tank had to be located in a hill with approximate dimensions as those reported in the paper, and no useful information was found by the authors in the literature. Three-dimensional finite elements models were built, in which the tank was located in three places,

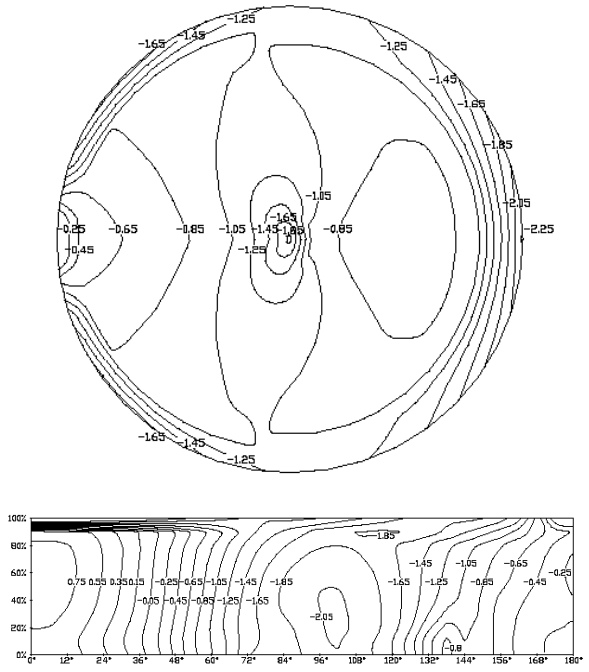

Figure 13. Cp distribution on the roof (a) and on the cylindrical walls (b) of an isolated tank .

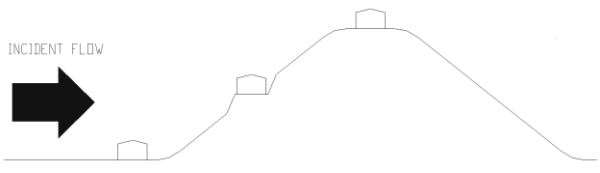

Figure 14 Locations of tanks in the hill investigated in this work.

Table 1: Summary of results for a tank in a hill.

Location of the tank	Range of pressure variation [kPa]
Top of the hill	26.72
Mid height	5.24
Bottom of the hill	2.70
Isolated	7.53

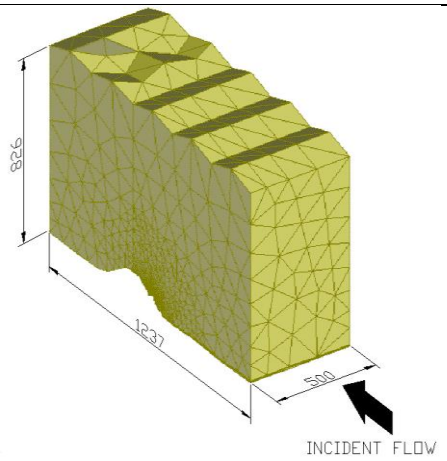

Figure 15a. Finite element mesh for a tank located at mid-height of the hill. The dimensions are in meters.

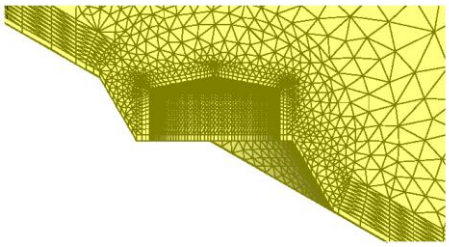

Figure15b. Detail of finite element mesh for a tank located at mid-height of the hill.

as shown in Fig. 14: (a) on flat terrain at the bottom of the hill; (b) on the slope at mid height of the hill; (c) at the top of the hill.

The most complex configuration to model was the second one, because it was necessary to define a flat surface on the slope of the hill, so that the tank could be realistically located. The circular plane used for the base had to be compatible with the slope in three dimensions. The angle for the local slope is 30º with respect to the vertical direction.

The finite element mesh adopted for the mid-height of the hill is shown in Fig. 15a, together with details of the discretization close to the hill and close to the tank (Fig. 15b). The finite element mesh was built using tetrahedral elements, with a total number of 47,689 elements and 22,065 nodes for case (a); 59,781 elements and 17,935 nodes for case (b); and 71,938 elements and 30,445 nodes for case (c).

The pressure distributions for the three locations with respect to the hill are shown in Figs. 16-18. In all cases, the same wind profile was imposed at the entrance of the control volume. To be able to compare the pressure patterns, the difference between maximum and minimum pressures are obtained, but the regions of vortex shedding were not considered for those computations. This range of pressure variation is important and independent of Reynolds number. The results are summarized in Table 1.

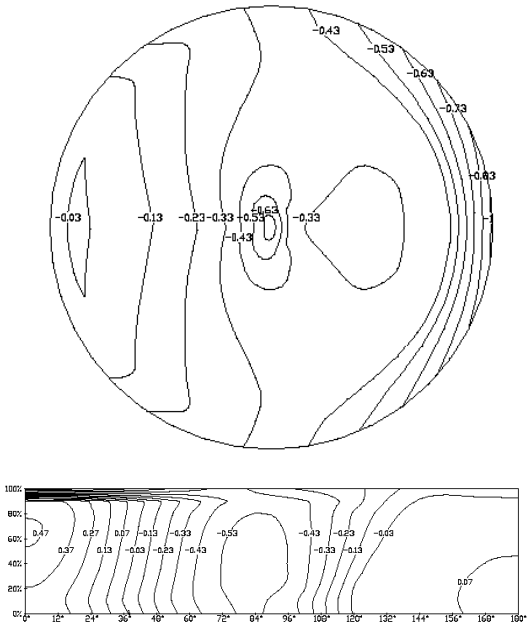

Figure 16. Cp distribution on the roof (a) and on the cylindrical walls (b) of a tank located at the base of the hill.

As expected, the worse location is the top of the hill, whereas the most favorable location is the base of the hill. An interesting behavior is obtained for the flow around the tank located at mid-height of the hill; here the flow separates at the entrance of the roof and does not go back to the tank, as it does in tanks at other locations with respect to the hill. The stream lines for this case are shown in Fig. 19.

The flows around tanks located either in isolated terrain or in different positions in a hill, computed in this paper, all have a common feature. The incident flow that impacts on the windward meridian of the tank leaves that zone in part by ascending and in part by surrounding the structure.

The flow that surrounds the tank is similar to what is expected in an infinitely long vertical cylinder: the flow remains attached to the surface up to half the circumference of the tank and then it breaks apart to induce a low energy flow on the leeward region of the structure. The part of the flow that ascends breaks apart from the structure at the intersection between the cylinder and the roof, and returns to the surface of the structure just at a small distance inside the roof, and remains attached to the roof all the way to the back of the tank roof. This is hown in Figures 13, 16, and 18. In the leeward zone, at the intersection between the roof and the cylindrical shell, two flows are superimposed: one coming from the roof and another one with low energy that surrounds the cylinder. This gives rise to the formation of highly localized vortex structures with low pressures.

The flow of the tank located at mid-height along the hill (Fig. 17) is different, because the flow that impacts and ascends on the windward zone breaks apart at the junction between the cylinder and the roof and never returns to the roof. This occurs because the flow in which the tank is immersed runs parallel to the surface of the

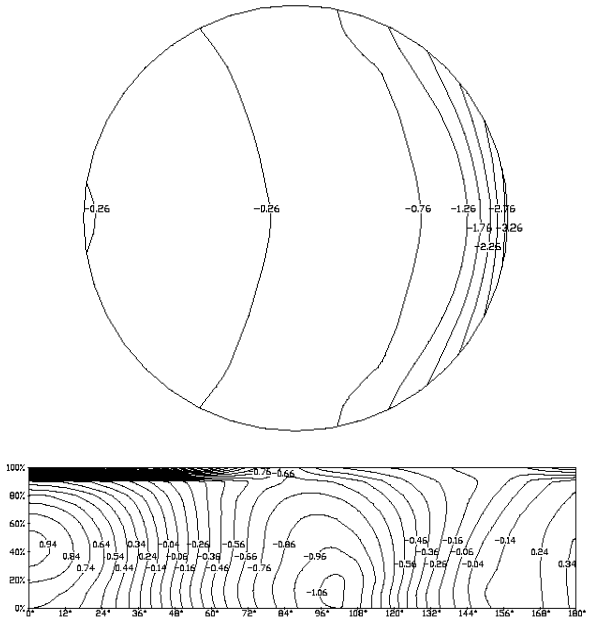

Figure 17. Cp distribution on the roof (a) and on the cylindrical walls(b) of a tank located at mid-height of the hill.

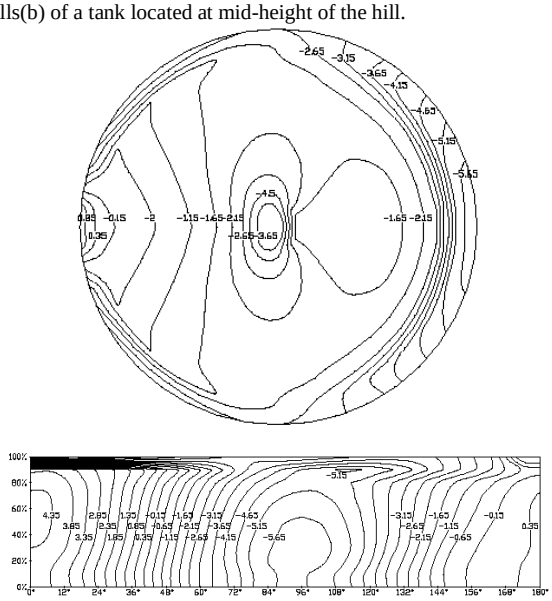

Figure 18. Cp distribution on the roof (a) and on the cylindrical walls (b) of a tank located at the top of the hill.

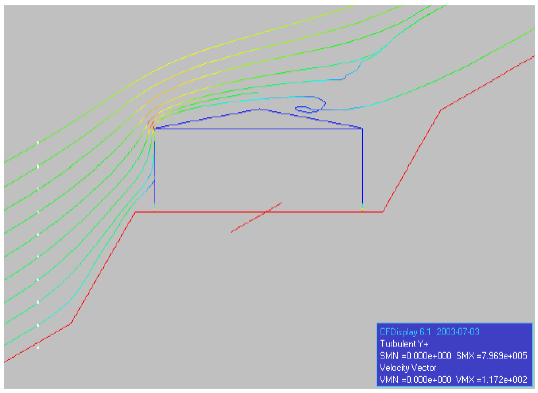

Figure 19. Stream lines at the plane of symmetry of a tank located at mid-height of the hill.

hill, so that the tank has a relative angle of 30º with respect to the direction of the flow. Furthermore, flow interaction does not occur at the back of the tank (as it does in tanks located at other places in a hill), and the leeward zone is characterized by low energy.

VII. CONCLUSIONS

Pressures in cylindrical tanks with a conical roof due to wind have been investigated in this paper using CFD. The tanks were assumed to be rigid, and the specific features of interest were the influence of topography on pressures. Such information if crucial to proceed with the structural analysis and design of tanks, and has been investigated in this paper because there are severe limitations in the information provided by wind-load provisions. From the results presented in the paper, several conclusions can be made:

(1) A hill obstructing the flow has a strong influence on the pressure profile affecting structures located in the hill. This was also predicted by the ASCE provisions; however, it was found in this work that the pressures depend on the specific geometry of the hill, including the dimensions and radius of curvature of the top flat part of the hill, and not just on the slope and height of the hill. Furthermore, the current provisions do not represent an upper bound to the pressures, so that it is suggested that a careful design of tanks may require a detailed study taking the local topography into account.

(2) The actual location of the tank with respect to the hill has a large influence on the pressures acting on the tank. For the case considered in this paper, a tank located on top of a hill would have pressure coefficients of the order of three times those acting on an isolated tank in flat terrain.

(3) For other locations at the base and mid-height of the hill, a decrease in pressure coefficients is observed with respect to the isolated tank. The reason for this is that the flow on the sides of the tank at mid-height of the hill has much less energy than in the isolated tank, because of the shielding effect produced by the flat surface on which the tank is supported. However, the maximum pressures in the windward meridian in the structure located at mid-height in the hill (Cp = 0.94) are larger than those in the isolated tank (Cp = 0.75), as shown in Figures 13b and 17b, because there is no shielding for that part of the tank.

(4) Not just the values but the pressure distributions depend on the location. This shows that the results cannot be easily extrapolated for other topographic conditions, tank locations and sizes.

(5) From the comparison of dynamic pressures, it is found that the values obtained in this research are somehow higher than those given by the ASCE provisions, with differences in the order of 5%.

ACKNOWLEDGEMENTS

The authors acknowledge the support of the Science and Technology Research Council of Argentina (CONICET), and the National University of Cordoba (SECYT-UNC) in the form of grants supporting this investigation.

REFERENCES

ASCE 7, *Minimum Design Loads for Buildings and Other Structures*, American Society of Civil Engineers, Reston, VA (2006).

Bergeles, G.C. "Numerical calculation of turbulent flow around two-dimensional hills," *Journal of Wind Engineering and Industrial Aerodynamics*, **21**, 307-321 (1985).

Bitsuamlak, G., T. Stathopoulos and C. Bedard, "Effects of upstream two-dimensional hills on design wind loads: A computational approach," *Wind and Structures*, **9**, 37-58 (2006).

Brun, E.A., A. Martinot-Lagarde and J. Mathieu, *Mécanique des Fluides*, **2**, Dunod, Paris (1959).

Cheung, J.C.K. and W.H. Melbourne, "Turbulence effects on some aerodynamic parameters of a circular cylinder at supercritical Reynolds number," *Journal of Wind Engineering and Industrial Aerodynamics*, **14**, 399-410 (1983).

CFDesign. Solver Technical Reference, Blue Ridge Numerics, Charlottesville, VA, USA (1999).

Falcinelli, O.A. *Estudio numérico de la acción de vientos sobre tanques y silos*, Tesis de Maestría en Ciencias de la Ingeniería – mención Aeroespacial, Universidad Nacional de Córdoba e Instituto Universitario Aeronáutico (2004).

Falcinelli, O.A., S.A. Elaskar, L.A. Godoy and J. Tamango, "Efectos de viento sobre silos y tanques mediante CFD," *Mecánica Computacional*, **21**, 256-273 (2002).

Falcinelli, O.A., S.A. Elaskar and L.A. Godoy, "Estudio mediante CFD de la influencia de la topografía en las cargas por viento sobre tanques," *Mecánica Computacional*, **22**, 161-170 (2003).

Finnigan, J.J. and R.A. Longstaff, "A wind tunnel model of forced convective heat transfer from cylindrical grain storage bins," *Journal of Wind Engineering and Industrial Aerodynamics*, **10**, 191-211 (1982).

Godoy, L.A., E.M. Sosa and G. Portela, "Nonlinear dynamics and buckling of steel tanks with conical roof under wind," *Thin-Walled Structures* (Ed. J. Loughlan), Institute of Physics Publishing, Bristol, UK, 407-414 (2004).

Holroyd, R.J. "On the behaviour of open-topped oil storage tanks in high winds. Part I. Aerodynamic aspects," *Journal of Wind Engineering and Industrial Aerodynamics*, **12**, 329-352 (1983).

Jackson, P.S. and J.C.R. Hunt, "Turbulent wind flow over a low hill," *Quarterly Journal of the Royal Meteorological Society*, **101**, 929-955 (1975).

Kim, H.G., V.C. Patel and C.M. Lee, "Numerical simulation of wind flow over hilly terrain," *Journal of Wind Engineering and Industrial Aerodynamics*, **87**, 45-60 (2000).

Lemelin, D.R., D. Surry and A.G. Davenport, "Simple approximations for wind speed-up over hills," *J. Wind Engineering and Industrial Aerodynamics*, **28**, 117-127 (1988).

Lun, Y.F., A. Mochida, S. Murakami, H. Yoshino and T. Shirasawa, "Numerical simulation of flow over topographic features by revised k– models," *Journal of Wind Engineering and Industrial Aerodynamics*, **91**, 231-245 (2003).

Macdonald, P.A., K.C. Kwok and J.D. Holmes, "Wind loads on circular storage bins, silos and tanks: I. Point pressure measurements on isolated structures," *Journal of Wind Engineering and Industrial Aerodynamics*, **31**, 165-188 (1998).

Macdonald, P.A., J.D. Holmes and K.C.S. Kwok, "Wind loads on circular storage bins, silos and tanks. II. Effect of grouping," *Journal of Wind Engineering and Industrial Aerodynamics*, **34**, 77-95 (1990a).

Macdonald, P.A., J.D. Holmes and K.C.S. Kwok, "Wind loads on circular storage bins, silos and tanks III. Fluctuating and peak pressure distributions," *Journal of Wind Engineering and Industrial Aerodynamics*, **34**, 319-337 (1990b).

Maher, F.J., "Wind loads on dome-cylinders and dome-cone shapes," *ASCE Journal of Structural Division*, **92**, 79-96 (1966).

Mulhearn, R.J., H.J. Banks, J.J. Finnigan and P.C. Annis, "Wind force and their influence on gas loss from grain storage structures," *J. Stored Products Res.*, **12**, 129-142 (1976).

Portela, G. and L.A. Godoy, "Wind pressures and buckling of aboveground steel tanks with a conical roof," *Journal of Constructional Steel Research*, **61**, 786-807 (2005a).

Portela, G. and L.A. Godoy, "Shielding effects and buckling of steel tanks in tandem arrays under wind pressures," *Wind and Structures: An International Journal*, **8**, 325-342 (2005b).

Purdy, D.M., P.E. Maher and D. Frederick, "Model studies of wind loads on flat-top cylinders," *ASCE Journal of Structural Division*, **93**, 379-395 (1967).

Sosa, E.M. and L.A. Godoy, "Non-linear dynamics of above-ground thin-walled tanks under fluctuating pressures," *Journal of Sound & Vibration*, **283**, 201-215 (2005).

Taylor, P.A. "Turbulent boundary-layer flow over low and moderate slope hills," *Journal of Wind Engineering and Industrial Aerodynamics*, **74-76**, 25-47 (1998).

Received: September 8, 2010
Accepted: November 29, 2010
Recommended by subject editor: Eduardo Dvorkin